Annales Geophysicae (2004) 22: 2625–2632
SRef-ID: 1432-0576/ag/2004-22-2625

Annales Geophysicae

Spatial and temporal properties of AKR burst emission derived from Cluster WBD VLBI studies

R. L. Mutel, D. A. Gurnett, and I. W. Christopher

University of Iowa, Iowa City IA 52242, USA

Received: 4 October 2003 – Revised: 30 March 2004 – Accepted: 5 May 2004 – Published: 14 July 2004

Part of Special Issue "Spatio-temporal analysis and multipoint measurements in space"

Abstract. We have determined the locations of over 6000 individual auroral kilometric radiation (AKR) bursts between July 2002 and May 2003 using a very long baseline interferometer (VLBI) array. Burst locations were determined by triangulation using differential delays from cross-correlated Cluster WBD waveforms. Typical position uncertainties are 200–400 km in the plane normal to the source-spacecraft line, but much larger along this line. The AKR bursts are generally located above the auroral zone with a strong preference for the evening sector (22:00 MLT ± 2 h). However, a few epochs imaged during the austral summer have loci in the daytime sector, especially near 15:00 MLT. There is marginal evidence for a small N-S hemispheric asymmetry in mean MLT and invariant latitude.

Key words. Magnetospheric physics (auroral phenomena) – Radio science (interferometry) – Space plasma physics (instruments and techniques)

1 Introduction

Auroral kilometric radiation (AKR) is an intense, narrowband terrestrial radio emission which occurs in short-duration bursts at frequencies between 50–800 kHz. It originates between altitudes 1–3 R_E above the Earth's surface along magnetic field lines threading the auroral zones (Gurnett, 1974; Kurth et al., 1975; Huff et al., 1988). The emission mechanism is thought to be an electron-cyclotron maser mechanism (Wu and Lee, 1979) which radiates at the local (relativistic) electron cyclotron frequency and whose free energy is likely derived from a unstable electron "shell" instability in regions of depleted electron density (Ergun et al., 1998, 2000). AKR emission is well correlated in intensity and frequency of occurrence with magnetospheric activity (Kurth and Gurnett, 1998; Liou et al., 2000), and with season (Kumamoto et al., 2003). Although a statistical association with auroral activity and especially with discrete auroral arcs has been reported (Gurnett, 1974; Benson and Akasofu, 1984), the exact locations of individual AKR bursts have been difficult to measure except by in situ observations of isolated regions (e.g., Hilgers et al., 1991; Louarn et al., 1990; Roux et al., 1993; Ergun et al., 1998).

In this paper we describe a novel direction-finding technique which can locate individual AKR burst locations over the entire auroral oval with unprecedented temporal and spatial resolution. We simultaneously record individual AKR bursts using the University of Iowa Wideband Data (WBD) receivers on the four Cluster spacecraft. We cross-correlate AKR burst waveforms from each pair of spacecraft to determine the burst time of arrival differences. By using the differential time delays on all baselines, the 3-dimensional location of individual bursts can be determined by triangulation. The technique is a restricted application of the well-known, very long baseline interferometry (VLBI) technique of conventional radio astronomy in that the independent WBD receivers are phase coherent and the received electric field waveforms are cross-correlated after correction for geometrical delay on each baseline. However, we utilize only the resulting differential time delays to determine source locations and not the interferometer phases. We also do not Fourier invert the measured visibilities to deduce source structure (AKR bursts are coherent, and are completely unresolved (Baumback et al., 1986)).

2 Summary of differential delay triangulation technique

The WBD instrument (Gurnett et al., 1997) consists of four identical receiver-antenna systems with receiver passbands of 12 kHz centered at 131, 256, and 506 kHz. The data are 8-bit digitized at a sample rate of 37 μs per sample and transmitted in real-time to separate ground receiving stations. Each data stream is time-stamped to an accuracy of less than 20 μs. The data streams from each pair of spacecraft are

Correspondence to: R. L. Mutel
(robert-mutel@uiowa.edu)

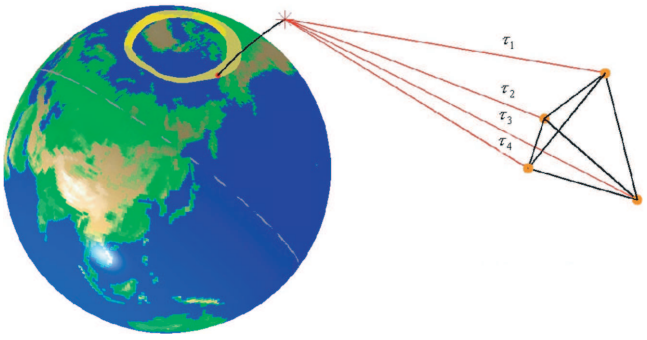

Fig. 1. Geometry of AKR source location algorithm using a 4-element VLBI array. The source location is found using geometric delays τ_j which are determined using the observed differential delays τ_{ij} and Eq. (1).

cross-correlated after correcting for propagation delays and the resulting cross-correlation function (CCF) is searched for significant peaks. The uncertainty in CCF peak measurements, $\delta\tau \sim 0.3$ ms, is determined by the width of the delay peak, which is the reciprocal of the average AKR burst bandwidth.

The geometry of the source location algorithm is shown in Fig. 1. The source location of an individual AKR burst $\boldsymbol{r}$ is related to the observed differential delays τ_{ij} measured at spacecraft locations s_i and s_j by

$$\tau_{ij} = \tau_j - \tau_i = \frac{1}{c} \cdot \left(|\boldsymbol{r} - \boldsymbol{s}_j| - |\boldsymbol{r} - \boldsymbol{s}_i| \right) \qquad i, j = 1, 4 \,.$$

In order to isolate emission from individual AKR bursts, the received waveform is filtered in time and frequency. A "data window" consists of a 300 ms x 1 kHz filtered waveform from each spacecraft.

Sample dynamic spectra and a data filtering window are shown in Fig. 2. Figures 2a–d show 30-s dynamic spectra from the all four spacecraft for an observation on 10 August 2002, beginning at 07:31:39 UT in the 250 kHz band. Figure 2e shows a magnified view of a section of the dynamic spectrum for spacecraft C3, with a black box indicating the 1 kHz × 0.3 s data window used for filtering each waveform before cross-correlation. Note that the bandwidth and time scale of the data window approximately matches the AKR instantaneous bandwidth and variability time scale of the AKR burst.

In searching for AKR burst locations, we searched all matching data window on each baseline for significant cross-correlation peaks over a range from -35 ms to $+35$ ms in steps of 0.1 ms. This is a compute intensive task, since we cross-correlated every data windows for each of six baselines, and there are 840 000 data window pairs per hour of observation. Finally, we filtered the resulting CCF delay peaks for location consistency by computing the signed sum of delays for each baseline triangle. This sum must be zero within the delay uncertainties on all four baseline triangles for a valid position solution.

Figure 2f shows the Cluster configuration in the sky plane as viewed from the AKR location. Since the spacecraft array is angularly well separated for this observation, some details of the AKR burst emission are significantly different (or even absent) when comparing spectra, especially for the largest separations (e.g., C1 vs. C4). This implies that the instantaneous beam pattern of AKR bursts is starting to be resolved by the largest spacecraft angular separation. We are presently analyzing this effect to determine the statistical properties of AKR beaming[1].

2.1 Position uncertainties

Since the Cluster constellation consists of four spacecraft, there are six independent baselines, and hence six observable differential delays. Hence, the solution for the three unknown components of source location $\boldsymbol{r}$ are overdetermined and can be solved for by minimization. In practice, the component along the line of sight to the Cluster constellation center of mass is less well constrained than the orthogonal coordinates. Since the spacecraft positions are known to an accuracy of less than 10 km (<0.03 ms), the location uncertainty is dominated by the differential delay uncertainty (0.3 ms). For a baseline with projected length B, the uncertainties perpendicular and parallel to the line of sight z between the Cluster centroid and the AKR emission are given by (Mutel et al., 2003)

$$\delta x_{\perp} = (\frac{z}{B}) \cdot c\delta t$$

$$\delta x_{\parallel} = 2(\frac{z}{B})^2 \cdot c\delta t \,,$$

where B is the projected baseline length and δt is the delay uncertainty. Using typical values ($\delta z \sim 6\,R_E$–$12 R_E$, $B \sim 5000$ km–10 000 km, $\delta t \sim 0.3$ ms), the perpendicular position uncertainty is 380–1400 km at the AKR burst location. For a 2-dimensional array of baselines, the perpendicular uncertainty can be represented as an ellipse whose axial ratio is the baseline length ratio projected on the sky plane but rotated by 90°. When the uncertainty ellipse is mapped to the auroral zone at 100 km altitude (by following magnetic field lines threading the ellipse), it shrinks in size by a factor of 2–3 depending on observing frequency.

The uncertainty along the line of sight is much larger, 2600 km–42 000 km, providing very little constraint on the line of sight distance. In order to constrain the line of sight distance, we assume that the AKR emission originates at an altitude such that the electron gyrofrequency is equal to the observing frequency. This assumption derives from the hypothesis that AKR emission is an electron-cyclotron maser mechanism, which agrees very well both with detailed AKR emission models (Pritchett et al., 2002) and with in situ observations of physical conditions in the AKR source emission region (e.g., Ergun et al., 1998). We use the IGRF-2000

[1] Mutel et al., in preparation, 2004.

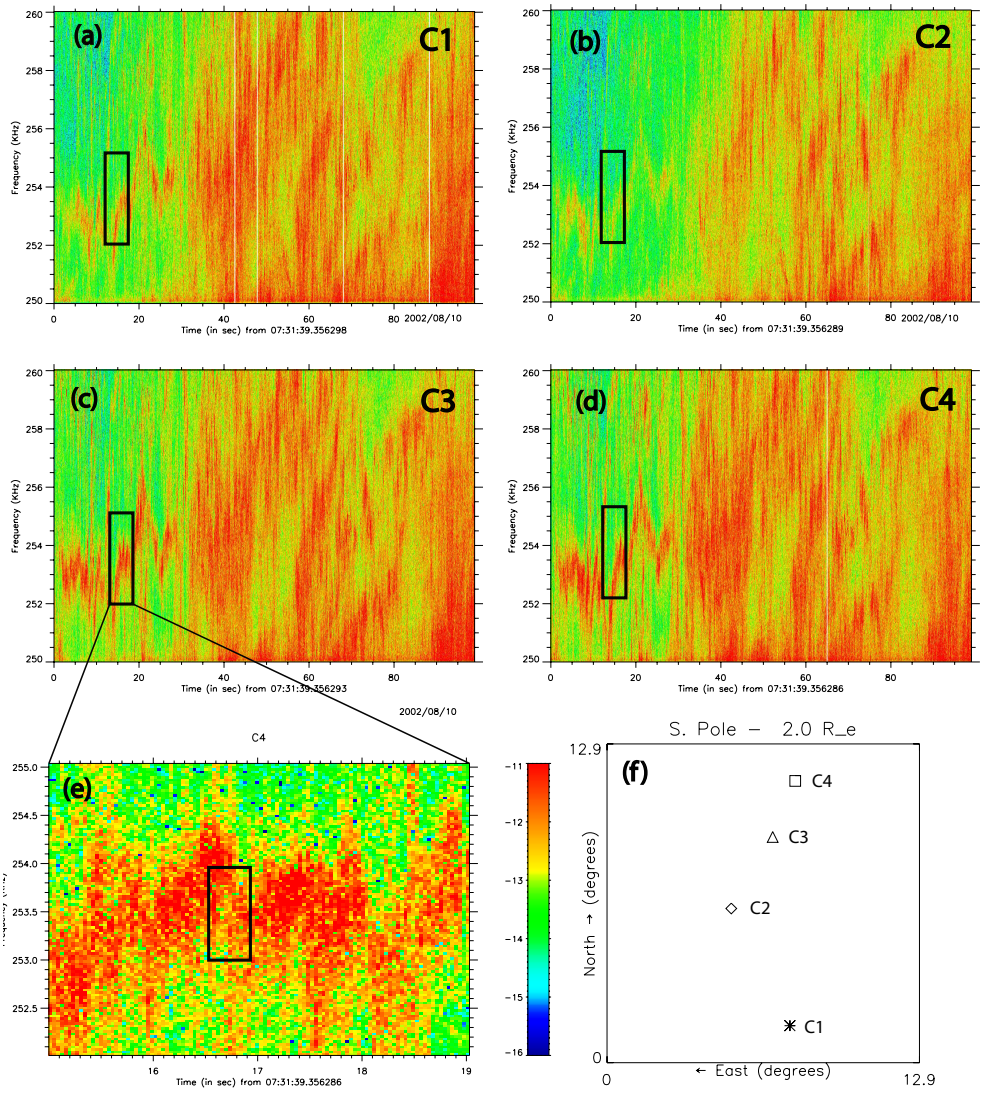

Fig. 2. (a)–(d) Dynamic spectra of AKR emission between 250 and 260 kHz received at spacecraft C1, C2, C3, and C4, respectively, on 10 August 2002 from 07:31:39 to 07:33:19 UT. **(e)** Magnified view of C3 dynamic spectrum (07:31:54.3 to 07:31:58.3 UT and 252 to 255 kHz). The black box (0.3 s×1 kHz) indicates a typical data window whose Fourier-filtered waveform is used for cross-correlation. **(f)** Spacecraft configuration (angular coordinates) as seen from the AKR source. The intensity log scale is in units $\mathrm{W\,m^{-2}\,Hz^{-1}}$. Note that the two (angularly) closely spaced spacecraft C3 and C4 have nearly identical spectra, while those spaced farther apart (C1, C2) have significantly different spectra, indicating that the AKR emission beam has structure on angular scales at least as large as 10°.

(Barton, 1997) model to calculate the Earth's magnetic field and assign a 10% depth uncertainty to all locations.

Using the above uncertainties, we can calculate an uncertainty volume for each observed AKR burst. This is illustrated in Fig. 3, which shows the locations and uncertainty volumes of AKR bursts projected to 100 km altitude on 28 October 2002 from 10:41–11:06 UT. The uncertainty volumes for each AKR location are color coded by frequency: 125 kHz is red, 250 kHz band is green, and 500 kHz band is blue. The typical "footprint" uncertainty has a dimension of 200–40 km in the auroral zone, but isolated bursts far from the sub-Cluster footpoint have elongated uncertainty volumes.

2.2 Refractive ray bending

The algorithm for determining the location of the AKR bursts assumes a rectilinear propagation path between the source and each of the four spacecraft. However, ray bending will occur if the refractive index along the path significantly deviates from unity. In order to evaluate this effect quantitatively, we used the global plasmasphere model of Gallagher et al. (2000) to construct ray paths from representative AKR burst locations to Cluster spacecraft locations over a range of geomagnetic latitudes and distances. For low geomagnetic latitudes ($\lambda_m < 10°$) the excess delay can significantly affect the apparent source position, as shown in Fig. 4. The two ray paths labeled (a) and (b) are calculated between an AKR

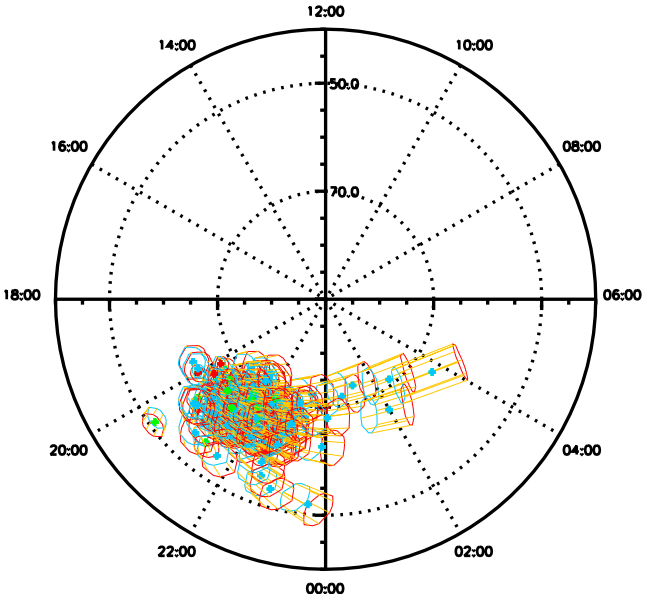

Fig. 3. Distribution of AKR burst locations and uncertainty ellipses in CGM coordinates for VLBI observations on 28 October 2003 from 10:41–11:06 UT. Frequency codes of the dots are red (125 kHz band), green (250 kHz band), and blue (500 kHz band); the projected cylindrical tapered prisms are the uncertainty volumes for each enclosed dot. The AKR burst locations are projected to 100 km altitude.

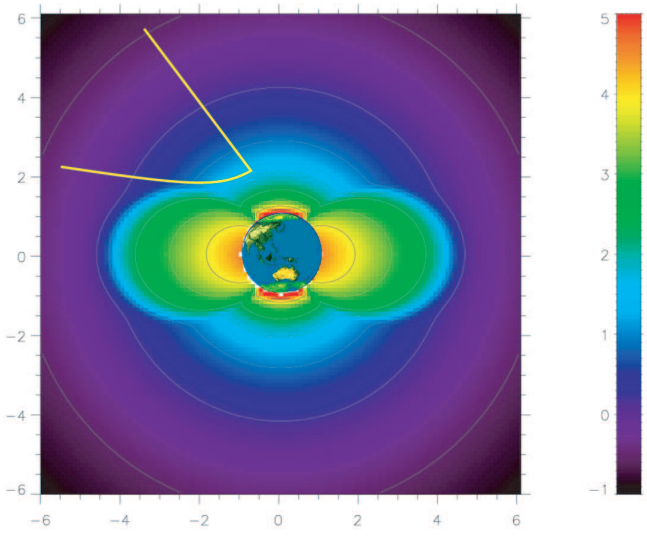

Fig. 4. Ray tracings for 250 kHz emission from a hypothetical AKR source at 2 R_E to spacecraft at 60° **(a)** and 10° **(b)** geomagnetic latitude. The plasmaspheric model, in pseudo-color coded electron density, (logarithmic levels), is from Gallagher et al. (2000) with geomagnetic index K_p=1.

source located at 2 R_E and 70° geomagnetic latitude, and a spacecraft located at 60° and 10°, respectively. The first ray is essential rectilinear while the second is bent through an angle ∼10°, a very significant shift relative to the delay uncertainty.

In Fig. 5 we show the excess path delay at all three observing frequencies compared with a rectilinear path. The excess path delay was determined for a low geomagnetic index (K_p=1) and for spacecraft distances of 10 and 13 R_E and satellite geomagnetic latitudes between 30° to 80°. This is a worst case scenario, since the plasmasphere is largest at low magnetic activity. Cluster VLBI data thus far have been acquired during low to moderate geomagnetic activity conditions ($1<K_P<4$). For spacecraft magnetic latitudes $\lambda_m>20°$ the excess delay is less than the delay uncertainty (0.3 ms). The total angular deviation from the unrefracted burst position (as viewed from the Cluster spacecraft) is ∼0.25° for these conditions, which corresponds to an apparent position shift ∼280 km at a spacecraft distance of 10 R_E, less than one resolution element. Hence, we have ignored refractive corrections to the calculated AKR source locations by restricting our analysis to observations taken when all four Cluster spacecraft were at magnetic latitudes $\lambda_m>20°$.

3 AKR burst locations

AKR emission is well-known to be narrow-band and bursty, with complex, short-duration drifting features (e.g., Gurnett, 1974; Benson et al., 1988). We have processed more than 50 epochs of 4-spacecraft VLBI observations, each of which has a duration between 1–3 h.

3.1 Single vs. multiple burst locations

Even when AKR emission is nearly continuous, only 1–2% of all data windows with detectable AKR emission provide acceptable position solutions, i.e., those for which the signed sum of differential delays on all baseline triangles are zero within the measurement uncertainty. There are several reasons why most cross-correlated data windows do not result in a unique location solution. First, all four spacecraft must be illuminated by the burst emission of an individual AKR burst. We have analyzed the beaming patterns of AKR bursts and find that only 10–30% of the bursts have instantaneous beaming sizes as large as the largest angular separations of the Cluster constellation (≳20°), as viewed from the AKR source location[2] instantaneous beam pattern of an AKR burst. Second, it is likely that many bursts are caused by multiple, spatially separated sources contributing to the same data windows. This would result in multiple cross-correlation delay peaks which would be rejected by our location-finding algorithm, which explicitly assumes a single AKR location for a given data window.

The single location constraint is a consequence of limited visibility sampling. Since the bursts are short in duration, we cannot take advantage of Earth-rotation synthesis to sample a range of visibilites for each baseline as with conventional VLBI (e.g., Thompson et al., 2001). Hence, only

[2] Mutel et al., in preparation, 2004.

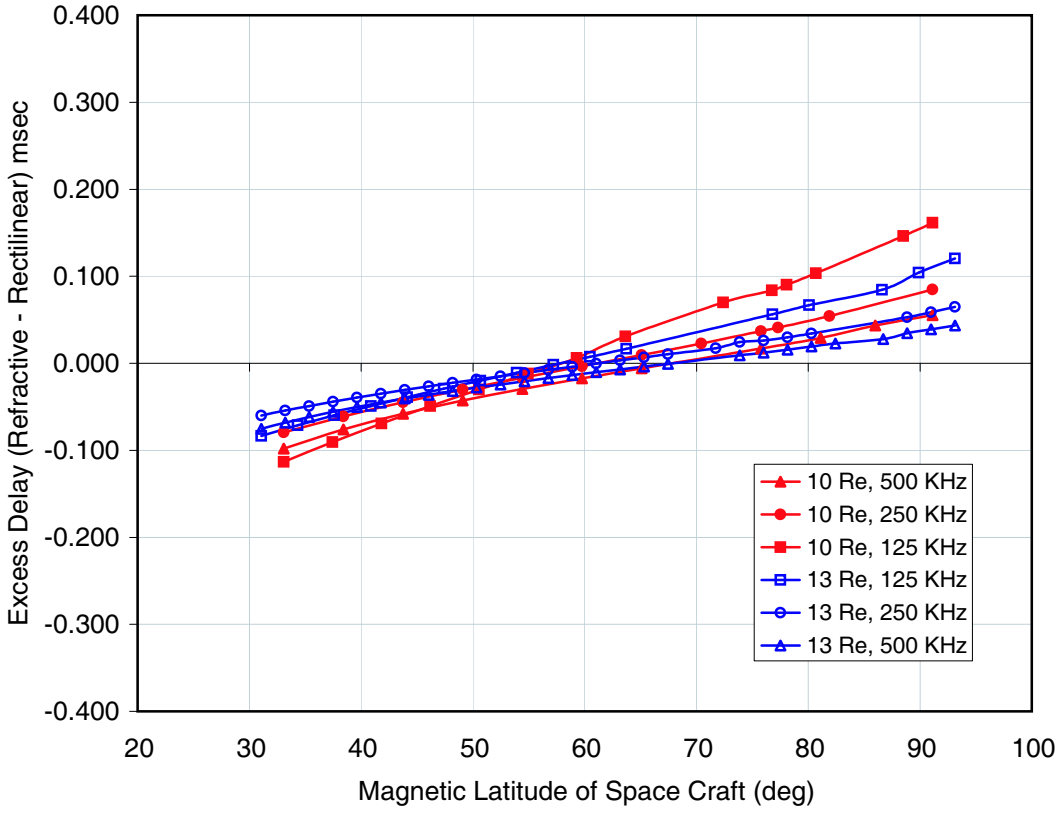

Fig. 5. Excess delay versus spacecraft magnetic latitude for AKR source-spacecraft distances of 10 R_E (red lines) and 13 R_E (blue lines) and frequencies of 125 kHz (△), 250 kHz (○), and 500 kHz (□).

six spatial frequencies are sampled in the complex visibility plane, so that at most only two independent point source positions could be determined. However, any such multiple source solution is non-unique, since there are many multiple-source locations which could produce the same six measured delays. Nevertheless, using the restricted criterion of only one cross-correlation peak per baseline, we have been able to locate more than 6000 individual burst locations and are now studying the resulting statistical properties of this data set.

3.2 Temporal characteristics

Figure 6 shows a montage of AKR source locations during a period of intense AKR emission on 9 November 2002 between 06:22 and 08:22 UT. Each sub-panel shows the location of all AKR bursts detected in the 15-minute interval centered on the labeled time. The lines connecting the AKR source region to the Earth trace the magnetic field through each source location. Although there is some variation on source centroid on a time scale of 15 min, the primary AKR source location is well constrained to a region whose magnetic footpoint is stationary at 21:00 MLT ±1 h and 70°±3° invariant latitude. This stationary behavior is typical for most epochs, although a few epochs show evidence for a systematic drift in CGM coordinates, corresponding to a drift speed of ∼80 kms^{-1} (Mutel et al., 2003).

3.3 Spatial characteristics

We are now investigating whether AKR burst locations vary systematically with hemisphere and with season. An intriguing, but tentative result, is shown in Fig. 7. Figure 7a shows the magnetic local time (MLT) distribution for 1955 AKR burst locations in the Northern Hemisphere (green line) and for 1644 locations in the Southern Hemisphere (red line), observed over the period from July 2002 to May 2003. Figure 7b is similar but for invariant magnetic latitude. Both data sets show that the large majority of AKR emission arises on magnetic fields lines threading the auroral zone in the evening sector, as found by previous authors using less direct methods (e.g., Kurth et al., 1975; Huff et al., 1988; Schreiber et al., 2002). However, there appears to be a marginally significant hemispheric difference in both mean MLT (20.8 MLT ±3.2 h N vs. 0.8 h ±3.2 h S) and invariant latitude (70.0°±4.7° N vs. 73.5°±5.7° S). We consider this result intriguing but tentative, and are presently analyzing a large number of additional epochs for additional confirmation.

To what extent is AKR emission coupled to auroral brightenings or discrete auroral arcs? Although a number of authors have claimed a statistical association largely on the basis of temporal coincidence (e.g. Gurnett (1974); Benson and Akasofu (1984); Hanasz et al. (2001)), the most direct

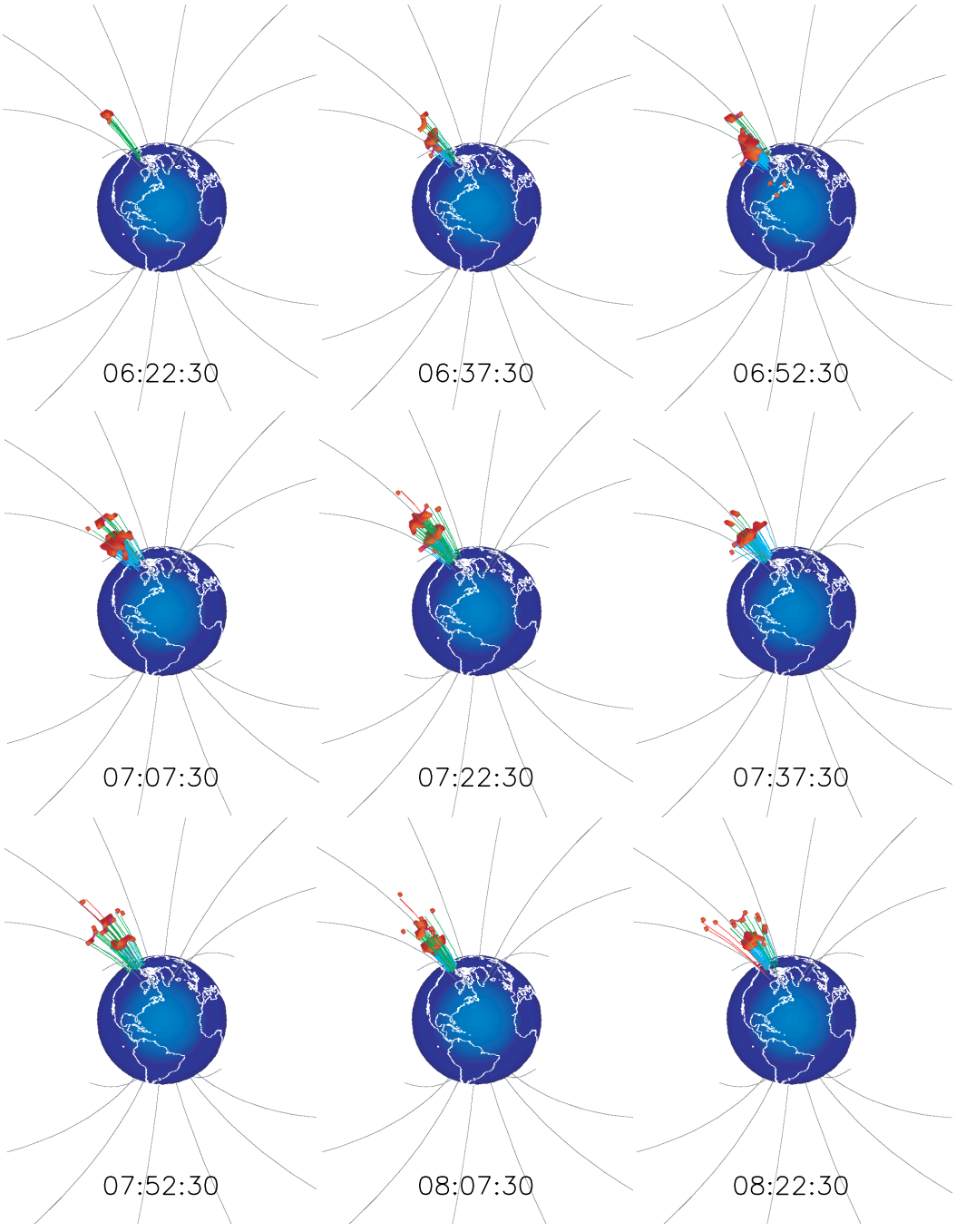

Fig. 6. Montage of AKR burst locations on 9 November 2002 between 06:22:30 and 08:22:30 UT. Subplots show individual AKR burst locations (0.3 s × 1 kHz data windows) in consecutive 15-min time intervals. Magnetic field lines connecting burst locations to the Earth's surface are shown as lines coded by AKR burst frequency (125 kHz red, 250 kHz green, 500 kHz blue).

evidence would entail simultaneous optical/UV imaging of the auroral oval with VLBI imaging of AKR burst locations. Unfortunately, we have not yet been able to schedule any 4-station Cluster observing epochs when there were simultaneous auroral images available from, for example, auroral imaging instruments on the POLAR or IMAGE spacecraft.

However, we have found several epochs in which AKR burst locations are above the auroral oval, but not in the evening sector, and which coincide with statistical auroral brightenings. For example, Liou et al. (1997) reported that the peak intensity of northern auroral oval emission near 1700 Å occurred near 22:00 MLT in April 1996 (spring in the Northern Hemisphere), but that there was a secondary dayside maximum near 15:00 MLT which dominated the monthly-averaged emission by July 1996 (arctic summer).

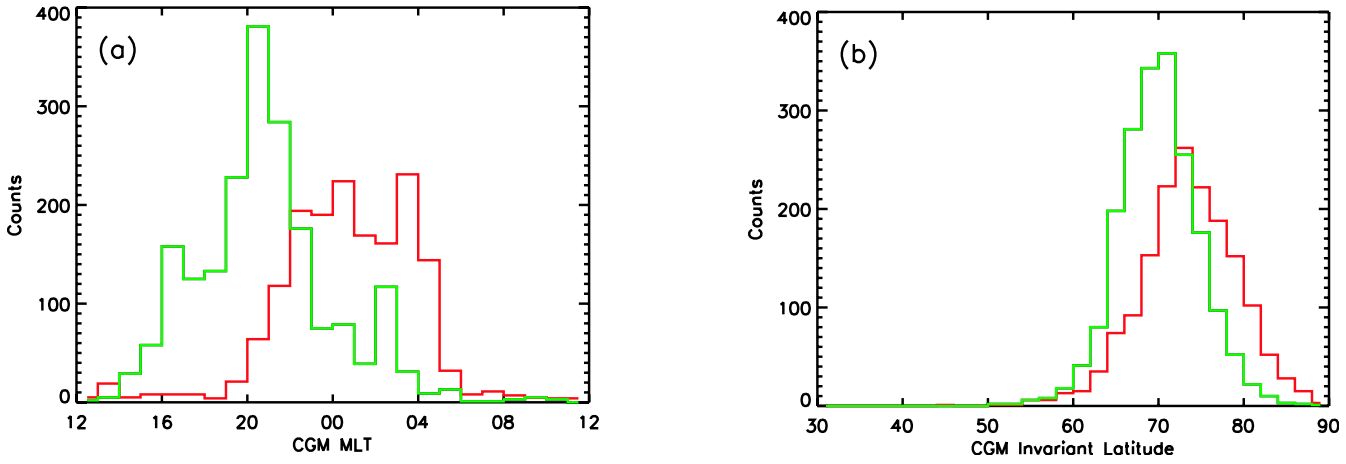

Fig. 7. **(a)** Histogram of the magnetic local time distribution of AKR burst locations in Northern Hemisphere (1955 bursts, green line) and Southern Hemisphere (1644 bursts, red line). **(b)** Same as (a), but for invariant magnetic latitude.

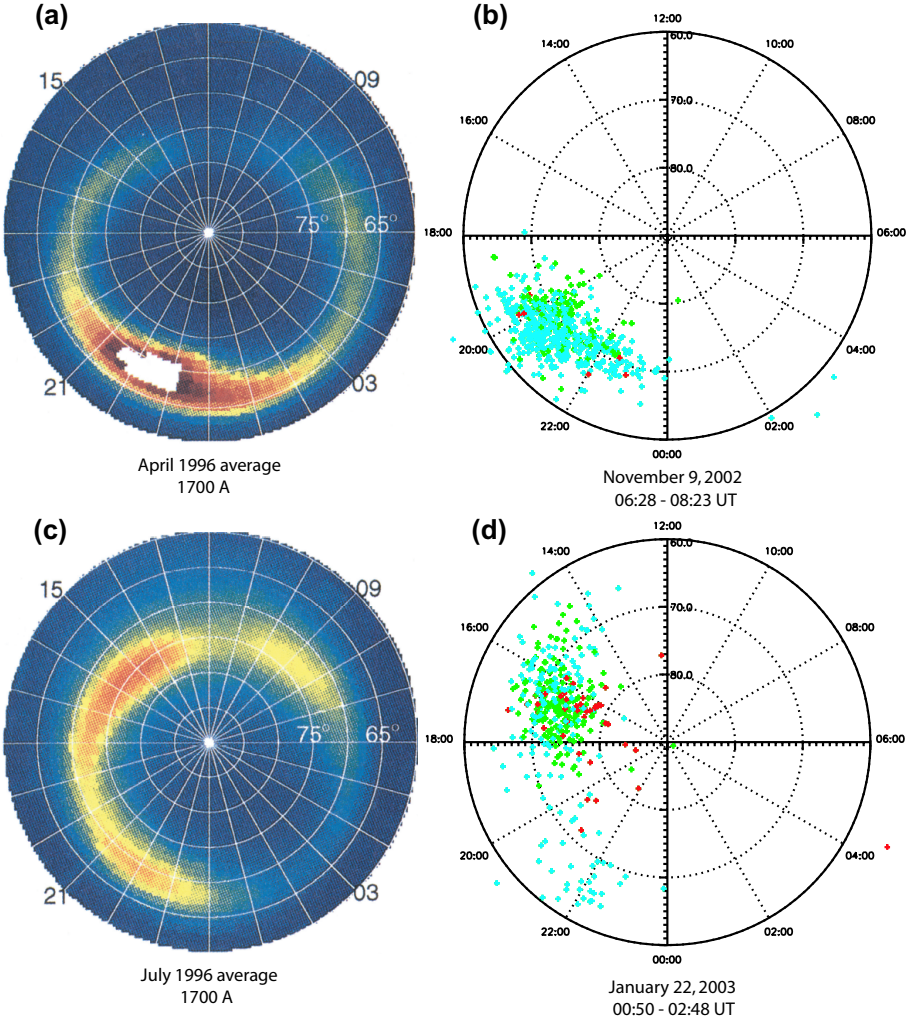

Fig. 8. **(a)** Monthly average map of UV (∼1700 Å) auroral emission in magnetic coordinates during April 1996 from Polar UVI imagery (Liou et al., 1997). **(b)** AKR burst emission locations on 9 November 2002 from 06:28–08:23 UT. The AKR locations are projected onto 100 km altitude by following magnetic field lines from each burst location. Frequency color coding is the same as in Fig. 3. **(c)** Same as (a) but for July 1996. **(d)** Same as (b) but for 22 January 2003 from 00:50–02:48 UT.

Figures 8a and c show the monthly-averaged Northern Hemisphere auroral maps of Liou et al. (1997) for these two seasons. We do not yet have sufficient observational data to construct corresponding monthly-averaged maps for AKR burst locations, but the initial map data support a spatial correspondence. Figures 8b and d show Southern Hemisphere AKR burst location maps at epochs 9 November 2002 (austral spring) and 22 January 2003 (austral summer), respectively. Although the auroral statistical map and the AKR epoch maps are clearly dissimilar in type and are not coeval, the spatial similarity is highly suggestive.

4 Summary

The VLBI differential delay technique provides a unique opportunity to directly measure the location of individual AKR burst locations with an uncertainty of 200–400 km at the magnetic footpoint. For the period from July 2002 to May 2003 we have observed more than 6000 AKR burst locations in the Northern and Southern Hemispheres. AKR source locations are generally above the auroral zone with a strong preference for the evening sector (22:00 MLT $\pm$2 h MLT but with some epochs clustered in the daytime sector, especially near 15:00 MLT). There is marginal evidence for a small N-S hemispheric asymmetry in mean MLT and invariant latitude, but this result is tentative and will require additional VLBI epochs to confirm.

Acknowledgements. Topical Editor T. Pulkkinen thanks two referees for their help in evaluating this paper.

References

Barton, C. E.: International Geomagnetic Reference Field: The Seventh Generation, J. Geomag. Geoelectr., 49, 123–148, 1997.

Baumback, M. M., Gurnett, D. A., Calvert, W., and Shawhan, S. D. : Satellite interferometric measurements of auroral kilometric radiation, Geophys. Res. Lett, 13, 1105–1108, 1986.

Benson, R. F. and Akasofu, S.-I.: Auroral kilometric radiation/aurora correlation, Radio Science, 19, 527–541, 1984.

Benson, R. F., Mellott, M. M., Huff, R. L., and Gurnett, D. A.: Ordinary mode auroral kilometric radiation fine structure observed by DE 1, J. Geophys. Res., 93, 7515–7520, 1988.

Ergun, R. E., Carlson, C. W., McFadden, J. P., Mozer, F. S., Delory, G. T., Peria, W., Chaston, C. C., Temerin, M., Elphic, R., Strangeway, R., Pfaff, R., Cattell, C. A., Klumpar, D., Shelly, E., Peterson, W., Moebius, E., and Kistler, L.: FAST satellite wave observations in the AKR source region, Geophys. Res. Lett, 25, 2061–2064, 1998.

Ergun, R. E., Carlson, C. W., McFadden, J. P., Delory, G. T., Strangeway, R. J., and Pritchett, P. L.: Electron-Cyclotron Maser Driven by Charged-Particle Acceleration from Magnetic Field-aligned Electric Fields, Astrophys. J. ,538, 456–466, 2000.

Gallagher, D. L., Craven, P. D., and Comfort, R. H.: Global Core Plasma Model, J. Geophys. Res.,105, 18 819–18 833, 2000.

Gurnett, D. A.: The earth as a radio source – Terrestrial kilometric radiation, J. Geophys. Res. ,79, 4227–4238, 1974.

Gurnett, D. A., Huff, R. L., and Kirchner, D. L. : The Wide-Band Plasma Wave Investigation, Space Science Reviews, 79, 195–208, 1997.

Hanasz, J., de Feraudy, H., Schreiber, R., Parks, G., Brittnacher, M., Mogilevsky, M. M., and Romantsova, T. V.: Wideband bursts of auroral kilometric radiation and their association with UV auroral bulges, J. Geophys. Res. ,106, 3859–3872, 2001.

Hilgers, A., Roux, A., and Lundin, R.: Characteristics of AKR sources – A statistical description, Geophys. Res. Lett ,18, 1493–1496, 1991.

Huff, R. L., Calvert, W., Craven, J. D., Frank, L. A. and Gurnett, D. A. : Mapping of auroral kilometric radiation sources to the aurora, J. Geophys. Res. ,93, 11 445–11 454, 1988.

Iijima, T. and Potemra, T. A. : Large-scale characteristics of field-aligned currents associated with substorms, J. Geophys. Res. ,83, 599–615, 1978.

Kumamoto, A., Ono, T., Iizima, M., and Oya, H.: Seasonal and solar cycle variations of the vertical distribution of the occurrence probability of auroral kilometric radiation sources and of upflowing ion events, J. Geophys. Res. Space Phys., 108, A1, 1032, doi:10.1029/2002JA009522, 2003.

Kurth, W. S., Baumback, M. M., and Gurnett, D. A.: Direction-finding measurements of auroral kilometric radiation, J. Geophys. Res., 80, 2764–2770, 1975.

Kurth, W. S. and Gurnett, D. A.: Auroral kilometric radiation integrated power flux as a proxy for A_E, Advances in Space Research, 22, 73–77, 1998.

Liou, K., Newell, P. T., Meng, C.-I., Brittnacher, M., and Parks, G.: Synoptic auroral distribution: A survey using polar ultraviolet imagery, J. Geophys. Res., 102, 27 197–27 205, 1997.

Liou, K., Meng, C.-I., Lui, A. T. Y., Newell, P. T., and Anderson, R. R.: Auroral kilometric radiation at substorm onset, J. Geophys. Res., 105, 25 325–25 332, 2000.

Louarn, P., Roux, A., de Feraudy, H., Le Queau, D., and Andre, M.: Trapped electrons as a free energy source for the auroral kilometric radiation, J. Geophys. Res., 95, 5983–5995, 1990.

Mutel, R. L., Gurnett, D. A., Christopher, I. W., Pickett, J., and Schlax, M.: Locations of Auroral Kilometric Radiation Bursts Inferred from Multi-Spacecraft Wideband Cluster VLBI Observations I: Description of Technique and Initial Results, J. Geophys. Res., 108(A11), 1398, doi:10.1029/2003JA010011, 2003.

Pritchett, P. L., Strangeway, R. J., Ergun, R. E., and Carlson, C. W.: Generation and propagation of cyclotron maser emissions in the finite auroral kilometric radiation source cavity, Journal of Geophysical Research (Space Physics), 107, A12, 1437, doi:10.1029/2002JA009403, 2002.

Roux, A., Hilgers, A., de Feraudy, H., Le Queau, D., Louarn, P., Perraut, S., Bahnsen, A., Jespersen, M., Ungstrup, E., and Andre, M.: Auroral kilometric radiation sources – In situ and remote observations from Viking, J. Geophys. Res. ,98, 11 657–11 670, 1993.

Schreiber, R., Santolik, O., Parrot, M., Lefeuvre, F., Hanasz, J., Brittnacher, M., and Parks, G.: Auroral kilometric radiation source characteristics using ray tracing techniques, Journal of Geophysical Research (Space Physics), 107, A11, SMP 20-1, CiteID 1381, doi:10.1029/2001JA009061, 2002.

Thompson, A., Moran, J., and Swenson, G. W.: Interferometry and Synthesis in Radio Astronomy, Second Edition, J. Wiley and Sons Publ., New York, 2001.

Wu, C. S. and Lee, L. C.: A theory of the terrestrial kilometric radiation, Astrophys. J., 230, 621–626, 1979.